Plasmonic Nanoantennas Enable Forbidden Förster Dipole-Dipole Energy Transfer and Enhance the FRET Efficiency

Juan de Torres,[†] Mathieu Mivelle,[‡] Satish Babu Moparthi,[†] Hervé Rigneault,[†] Niek F. Van Hulst,[‡,¶] María F. García-Parajó,[‡,¶] Emmanuel Margeat,[§,‖,⊥] and Jérôme Wenger[*,†]

CNRS, Aix-Marseille Université, Centrale Marseille, Institut Fresnel, UMR 7249, 13013 Marseille, France, ~~ICFO-Institut de Ciencies Fotoniques, Mediterranean Technology Park,~~ 08860 Castelldefels, Spain, ICREA-Institució Catalana de Recerca i Estudis Avançats, Barcelona, 08010, Spain, CNRS UMR5048, Centre de Biochimie Structurale, 29 rue de Navacelles, 34090 Montpellier, France, INSERM U1054, 34090 Montpellier, France, and Université Montpellier, 34090 Montpellier, France

E-mail: jerome.wenger@fresnel.fr

Abstract

Förster resonance energy transfer (FRET) plays a key role in biochemistry, organic photovoltaics, and lighting sources. ~~However, in addition to the short nanometer distance between~~

[*]To whom correspondence should be addressed
[†]Aix-Marseille University
[‡]ICFO
[¶]ICREA
[§]CNRS UMR5048
[‖]INSERM U1054
[⊥]Université Montpellier

donor and acceptor dyes, FRET also requires adequate mutual dipole orientation. The orientation dependence complicates the FRET analysis in biological samples and may even lead to the absence of FRET for perpendicularly oriented donor and acceptor dipoles. Here, we show how to exploit the strongly inhomogeneous and localized fields in plasmonic nanoantennas to open new energy transfer routes, overcome the limitations from the mutual dipole orientation, and ultimately enhance the FRET efficiency. The simultaneous presence of perpendicular near-field components in the nanoantenna sets favorable energy transfer routes that increase the FRET efficiency up to 50% for nearly perpendicular donor and acceptor dipoles. This new facet of plasmonic nanoantennas enables dipole-dipole energy transfer that would otherwise be forbidden in a homogeneous environment. It further increases the applicability of single molecule FRET over diffraction limited approaches, with the additional advantages of higher sensitivities and higher concentration range towards physiological levels.

Keywords FRET, plasmonics, LDOS, nanoantenna, fluorescence enhancement, dipole-dipole interaction

Förster resonance energy transfer (FRET) describes the near-field dipole-dipole energy exchange from an excited donor to a ground state acceptor emitter.[1,2] This phenomenon plays a key role in energy harvesting,[3–5] and is also widely used to probe molecular conformations and interactions.[6–9] A major feature of FRET is its highly sensitivity to the relative position of donor and acceptor fluorophores at the nanoscale, with the energy transfer efficiency going down with the inverse sixth power of the donor-acceptor distance.

In addition to the donor-acceptor distance, FRET is also highly dependent on the mutual orientation between the donor and acceptor transition dipoles.[10–13] The FRET efficiency is maximal when both dipoles are aligned, and is strictly zero for perpendicular dipoles, whatever the separation between them. This orientation dependence complicates the FRET analysis as the orientation mobility of the fluorophores is often constrained in biological samples and the hypothesis assuming isotropic orientation averaging is no longer valid.[10,11] It may even lead to the erroneous absence

of FRET detection for perpendicular donor and acceptor dipoles, despite their mutual presence on the construct and their nanometer separation.

Nanophotonic structures offer new ways to enhance light-matter interactions at nanoscale dimensions.[14,15] Several structures such as resonant microcavities,[16–18] plasmonic antennas,[19–25] or waveguides[26–29] have been considered to tailor the photonic environment so as to manipulate the energy transfer between dipole emitters. The FRET rate constant was shown to be barely affected by mirrors,[30–32] microresonators[33,34] and dielectric nanoparticles,[35,36] which do not provide enough field confinement. Plasmonic nanostructures such as nanoparticle arrays,[37–39] metal nanoapertures[40,41] and nanogap antennas[42,43] are the key to significantly enhance the FRET rate. ~~However, while~~ most of these works focus on the relationship between FRET and the local density of optical states (LDOS), ~~the~~ dipolar orientation in FRET has been largely overlooked so far. ~~Moreover, several works highlight the competition between FRET and the other radiative and nonradiative decay processes from the donor excited state, which generally leads to a decrease in the FRET efficiency.~~[30,42,43] Controlling this competition and enhancing the FRET efficiency have remained major challenges so far.

In this work, we show how the strongly inhomogeneous and localized fields in plasmonic nanoantennas can be used to open new energy transfer routes, overcome the limitations from the mutual dipole orientation, and ultimately enhance the FRET efficiency. Contrarily to the far field radiation of a dipole in a homogeneous medium which contains a single transverse component, the near field (evanescent) radiation of a dipole in a plasmonic nanoantenna has electric field components along all three directions of space. This simultaneous presence of perpendicular near-field components opens favorable energy transfer routes whatever the mutual orientation of the donor and acceptor dipoles. Our data show that the FRET efficiency can be enhanced up to 50% for nearly perpendicular donor and acceptor dipoles in a plasmonic nanogap antenna, with the FRET enhancement largely overcoming the losses and dominating the competition with the other decay processes from the donor excited state. This important result demonstrates that plasmonic nanoantennas enable the observation of dipole-dipole energy transfer that would otherwise be forbidden

because of near perpendicular orientation of the donor and acceptor dipoles. It emphasizes a new facet of optical nanoantennas and provides a strategy to use nanophotonics to reveal FRET interactions that would otherwise be challenging to probe using diffraction-limited microscopes.

The relative orientation between the donor and acceptor transition dipoles is generally described in FRET by the orientation parameter $\kappa^2 = (\cos\theta_T - 3\cos\theta_D \cos\theta_A)^2$, where θ_T is the angle between the donor and acceptor dipoles, and θ_D, θ_A are the angles between each dipole and the axis joining them (Fig. 1a).[11,44] κ^2 is maximal and amounts to 4 when both dipoles are aligned ($\theta_T = \theta_D = \theta_A = 0$), while κ^2 vanishes for dipoles in parallel planes with perpendicular orientation ($\theta_T = \theta_D = \theta_A = 90°$). Often the orientation-averaged value $\kappa^2 = 2/3$ is considered, assuming that both fluorescent dyes are freely mobile and that the isotropic reorientation occurs on a timescale much faster than the decay lifetime from the donor excited state. However, this assumption ~~may break~~ for situations where the orientation mobility of the fluorophores is constrained.[10,11]

Cy3 and Cy5 form a commonly used FRET pair that presents a clear mutual orientation dependence.[11] It has been shown that Cy3 and Cy5 predominantly stack on the ends of the DNA helix in the manner of an additional base pair when they are attached to the 5' termini of duplex DNA with short carbon linkers.[45–48] In this work, we use this phenomenon and select specific DNA constructs providing near perpendicular orientation between the Cy3 donor and Cy5 acceptor. With Cy3 and Cy5 being predominantly stacked to the 5' end of the DNA duplex, the relative orientation of the dipoles can then be tuned by adapting the length of the DNA double strand, as shown by the simulations on Fig. 1b.[11] DNA lengths of 12 and 17 base pairs are found optimal to provide near perpendicular orientation of the donor and acceptor dipoles. We confirm these predictions by experimental measurements of the FRET efficiencies in the confocal reference setup for the Cy3-Cy5 samples with 12 and 17 base pairs DNA lengths (red dots in Fig. 1b and Supporting Information Fig. S1 for the FRET efficiency histograms). These data show a significant ~~deviation from~~ the expected efficiency assuming the isotropic $\kappa^2 = 2/3$ orientation (further confirmed by ensemble spectroscopy measurements, see Supporting Information Fig. S2). From this ~~deviation~~, we compute back the orientation parameter κ^2 for each sample. For the Cy3-Cy5 sample with 12

base pairs separation (denoted Cy3-12-Cy5), κ^2 vanishes to 0.06 ± 0.03, indicating near perfectly perpendicular orientation of the dipoles. For the larger 17 base pairs separation (Cy3-17-Cy5 sample), κ^2 ~~increases~~ to 0.2 ± 0.1 ~~but remains still~~ significantly lower than the isotropic $2/3$ value. ~~A similar behavior was already observed,[11] and is related to a residual dynamic mobility of the fluorophores together with a minor fraction of Cy3 unstacked from the DNA.~~

To compare with a case ~~where~~ the orientation mobility of the fluorophores is not noticeably constrained, we select a Atto550-Atto647N FRET pair covalently linked to double stranded DNA with a flexible linker, and set a 20 base pair separation between the dyes (Fig. 1c).[40,41] For this sample, the measured FRET efficiency and the value $\kappa^2 = 0.6 \pm 0.2$ stand in good agreement with the orientation-averaged $\kappa^2 = 2/3$ hypothesis (Supporting Information Fig. S1), so that this construct can be used as a reference for freely mobile fluorophores. Moreover, as the absorption and emission spectra of cyanine and Atto FRET pairs are almost similar (Supporting Information Fig. S3), the results for both systems can be directly compared.

To probe the influence of the dipole-dipole orientation in FRET enhanced by photonic nanostructures, we use two different designs: a 20 nm gap nanoantenna between two 80 nm aluminum particles (Fig. 1d,e) and a circular aperture with 200 nm diameter (Fig. 1f,g). Both structures are milled by focused ion beam in an aluminum film, with 50 nm thickness for the nanogap antenna and 150 nm for the nanoaperture. The electromagnetic intensity is confined inside the nanogap region (Fig. 1e) and at the bottom of the nanoaperture (Fig. 1g), as indicated by the numerical simulations using finite difference time domain (FDTD) method. This confinement is further confirmed by fluorescence correlation spectroscopy (FCS) experiments to quantify the near field detection volume inside the nanostructures.[41,42]

The FRET experiments are performed on an inverted confocal microscope which enables to select individual nanostructures and record simultaneously the fluorescence emission dynamics for both the donor and acceptor dyes with picosecond resolution. Diluted concentrations of the FRET constructs ensure that the observations are performed at the single FRET pair level and avoid potential collective effects in FRET.[16,31] Fluorescence intensity time traces show bursts representing

a detection event of a single FRET pair diffusing across the nanoscale detection volume (Fig. 2a). Burst intensities are higher in the nanoantenna than in the nanoaperture or confocal reference (Supporting Information Fig. S4). This confirms the strong confinement of the electromagnetic energy much below the diffraction limit and ~~indicate~~ fluorescence enhancement.[41,42] For the nanoaperture, the fluorescence enhancement factors are $\eta_{F,d} = 5.4$ and $\eta_{F,a} = 5.75$ for isolated Cy3 and Cy5 terminally attached to double stranded DNA. For the nanogap antenna, we find $\eta_{F,d} = 10.6$ and $\eta_{F,a} = 7.8$ for isolated Cy3-DNA and Cy5-DNA constructs respectively.

~~The main result of our study is the comparison of~~ the FRET efficiency histograms for the different predominant orientations of the fluorescent dipoles and the different nanophotonic structures (Fig. 2b). For every detected fluorescence burst, the corresponding FRET efficiency E_{FRET} is computed from the ratio of intensities in the acceptor and donor channels. Our analysis carefully takes into account several phenomena, which are calibrated separately: the direct excitation of the acceptor by the laser light, the donor emission crosstalk into the acceptor channel, the differences in the quantum yields and detection efficiencies for the donor and acceptor emission and the fluorescence enhancement for the isolated donor and acceptor (see Methods section for details). The measured FRET efficiencies are stored in histograms and displayed in Fig. 2b for a direct comparison between the FRET constructs and the nanostructures. These histograms assess the occurrence of FRET by their non-zero mean values which clearly differ from the data recorded for the isolated Cy3 donor (Supporting Information Fig. S5).

For the Atto550-20-Atto647N sample with nearly complete fluorophore mobility, the average FRET efficiency is reduced by about two-fold as the experimental conditions move from the confocal to the nanoantenna (Fig. 2b, left column). This efficiency reduction ~~was already observed in~~ our earlier work,[42] and is related to the larger increase of the isolated donor total decay rate Γ_{Do} (mainly due to ohmic losses to the metal) as compared to the enhancement of the FRET rate Γ_{FRET}. This phenomenon contributes to lower the apparent FRET efficiency $E_{FRET} = \Gamma_{FRET}/(\Gamma_{FRET} + \Gamma_{Do})$ by increasing its denominator ratio.

A strikingly different evolution is observed for the Cy3-Cy5 samples with constrained fluo-

rophore mobility and near perpendicular dipole orientation (Fig. 2b, center and right columns). ~~The mean FRET efficiencies are further summarized in Fig. 2c. Despite identical nanophotonic LDOS conditions (and optical losses) as for the Atto550-20-Atto647N sample, the FRET efficiencies for the Cy3-12-Cy5 and Cy3-17-Cy5 samples are remarkably *increased* in the plasmonic nanostructures as compared to confocal.~~ The highest efficiency increase of more than 50% is obtained for the nanogap antenna and the Cy3-12-Cy5 sample bearing the smallest orientation parameter ($\kappa^2 = 0.06$). These results evidence the key role played by the mutual dipole-dipole orientation in nanophotonics-enhanced FRET, and demonstrate that the electromagnetic near-field control by the nanoantenna opens new energy transfer routes. These routes are especially valuable for FRET constructs with near perpendicular dipole orientation where the energy transfer is essentially prohibited in a homogeneous photonic environment. The simultaneous presence of evanescent fields along all space directions inside the nanoaperture and even more inside the nanogap antenna allows to overcome the limitations of mutual orientation and to set the local electromagnetic conditions so as to maximize the absorption by the acceptor dipole of the field generated by the donor dipole.

~~To confirm the observations of enhanced FRET efficiencies with fluorescence burst analysis,~~ we use time correlated single photon counting (TCSPC) as separate independent method to record the donor fluorescence lifetime and extract the mean FRET rate constant and FRET efficiency. The decay traces for the isolated Cy3 donor reveal faster emission dynamics in the antenna than in confocal or in the aperture (Fig. 3a), with a mean fluorescence lifetime reduction from 750 ± 40 ps for the confocal reference, to 550 ± 40 ps in the nanoaperture and 210 ± 20 ps in the nanogap antenna (all the parameters used for fitting the fluorescence decays are summarized in Supporting Information Tab. S1). This fluorescence lifetime reduction indicates a higher LDOS in the nanostructures. Using the calibrated 30% quantum yield of Cy3 attached to the 5' end of double stranded DNA,[49] the lifetime reduction can be corrected for the internal nonradiative decay rate to retrieve only the LDOS enhancement.[50] We measure LDOS enhancement of $2.2\times$ in the aperture and $10\times$ in the nanogap antenna, in good agreement with ~~earlier works~~ on high quantum yield Atto550 dyes.[41,42]

In the presence of the acceptor, the donor decay rate constant is further increased to $\Gamma_{DA} =$

$\Gamma_{Do} + \Gamma_{FRET}$ and includes the new decay rate constant Γ_{FRET} opened by the energy transfer. In all the experimental conditions, the presence of the acceptor further accelerates the donor emission dynamics with a larger impact when the separation is shorter (Fig. 3b). The different donor fluorescence lifetimes are summarized in Fig. 3c and Supporting Information Tab. S1. These are used to estimate the FRET rate constants $\Gamma_{FRET} = \Gamma_{DA} - \Gamma_{Do}$ (Supporting Information Fig. S6) which experience a clear enhancement in the nanostructures as compared to the confocal reference (Fig. 3d). The FRET rate enhancement grows from the aperture to the antenna case as the field is more confined, and a further increase is observed depending on the mutual orientation of the dipoles. We measure a 8-fold enhancement of Γ_{FRET} for the Cy3-12-Cy5 construct in the nanoantenna. This corresponds to the largest enhancement reported so far.[40–43] In comparison with the 3-fold enhancement obtained with the orientation-averaged Atto sample, the 8-fold value for Cy3-12-Cy5 reveals that the increase in the apparent orientation parameter κ^2 in the nanoantenna has a dominant contribution to the FRET rate enhancement.

Additionally, the average FRET efficiency can be computed based on the fluorescence lifetime data according to the relationship $E_{FRET} = 1 - \Gamma_{Do}/\Gamma_{DA}$. These latter values can be compared to the FRET efficiencies deduced from burst analysis (Supporting Information Fig. S7). Both independent methods converge towards similar values, and assess the occurrence of enhanced FRET efficiency inside the nanostructures for the constructs with near perpendicular dipole orientation.

Numerical simulations illustrate the influence of the electric field polarization at the nanoscale and explain the enhanced FRET efficiency (Fig. 4). A quasi-classical description of the dipole-dipole energy transfer shows that the FRET rate constant Γ_{FRET} scales as the donor power transferred to the acceptor.[44] This power is proportional to the square of the electric field emitted by the donor at the acceptor position projected on the acceptor's dipole axis $|\mathbf{n}_\mathrm{A} \cdot \mathbf{E}_\mathrm{D}(\mathbf{r}_\mathrm{A})|^2$. In the near-field and in a homogeneous environment, a radiating electric dipole has both transverse and longitudinal components. However, in spherical coordinates its azimuthal (φ angle) component remains strictly zero.[44] This also explains why perpendicularly oriented dipole do not exchange energy by FRET whatever the separation between them. To reproduce this condition and to inves-

tigate the antenna's influence, we compute the azimuthal component for a radiating electric dipole in free space using FDTD and indeed find a vanishing electric field amplitude (Fig. 4a-d, the field amplitude is magnified by 100× to ease viewing). In contrast, the field component projected onto the azimuthal axis is no longer zero in the presence of the nanoantenna which breaks the homogeneous environment assumption and couples the different electric field components radiated by the dipole (Fig. 4e-h). Inside the gap of the nanoantenna, the electric field component projected along the azimuthal direction (parallel to the acceptor dipole) can be enhanced by up to a thousand fold. This electric field then enables the energy transfer to the acceptor that would otherwise be prohibited in a homogeneous environment. Since the FRET rate constant scales as the square power of the electric field amplitude, the FRET rate can thus be up to one million fold larger for this specific configuration.

Metal nanoapertures and plasmonic antennas generate strongly inhomogeneous and localized near fields. For a single emitter, these properties have led to the demonstrations of giant fluorescence enhancement,[51–54] ultrafast picosecond lifetime,[55–57] directional emission,[58] photobleaching reduction,[59,60] and single molecule detection at high concentrations.[61,62] For two emitters and FRET, the nanophotonic structures bring three important ~~supplementary~~ effects. First, the confinement of the electromagnetic field to nanoscale distances of the order of the donor-acceptor separation enhances the FRET rate ~~constant~~, as measured here and ~~already~~ pointed out in earlier works.[42,43] Second, the higher LDOS in the plasmonic structures accelerates the other radiative and nonradiative decay processes from the donor excited state, which compete with FRET and tend to reduce its efficiency.[30,34] Third – this is the main conclusion of this work – the strongly inhomogeneous and localized fields in the plasmonic nanostructures have components along all the three space directions, which can be used to open efficient energy transfer routes between the dipoles. Importantly, this FRET enhancement can largely overcome the losses and dominate the competition with the other decay processes contributing to the LDOS. As a result, FRET can be allowed even for perpendicularly oriented donor-acceptor pairs.

In conclusion, we have reported that the strongly inhomogeneous and localized fields in plas-

monic nanoantennas can open new energy transfer routes, overcome the limitations from the mutual dipole orientation, and ultimately enhance the FRET efficiency up to 50% for nearly perpendicular donor and acceptor dipoles. These results are important since they indicate that optical antennas can extend the applicability of FRET to conditions where dipole-dipole interactions would otherwise be too weak to result in a detectable FRET signal. Additionally, our nanoantenna and nanoaperture designs are fully compatible with the detection of single molecules in solution at physiological micromolar concentrations.[61,62] This provides a supplementary improvement of confocal microscopes to bring single molecule FRET towards higher physiological concentrations and higher sensitivities.

Methods

Antenna fabrication. Nanoapertures and nanoantennas are milled by focused ion beam (Zeiss Auriga 60 FIB-SEM, 1 nm resolution GEMINI SEM, equipped with Orsay Optics 2.5 nm resolution Cobra ion column) on respectively 150 nm and 50 nm thick aluminum films deposited by thermal evaporation (Oerlikon Leybold Univex 350). The aperture diameter is 200 nm. For the antenna, the inner particle diameter is 80 nm with gap size of 20 nm, while the surrounding aperture dimensions are 300x100 nm^2.

DNA samples. Double-stranded DNA constructs of 12 and 17 base pair length sequences are designed with one Cy3 donor on the forward strand, and one Cy5 acceptor on the reverse strand and are similar to the ones used in.[11] The DNA sequences for the Cy3-12-Cy5 sample are:

Cy3-5'-CCACTGGCTAGG-3',

Cy5-5'-CCTAGCCAGTGG-3'.

The DNA sequences for the Cy3-17-Cy5 sample are:

Cy3-5'-CCACTGCACCTGCTAGG-3',

Cy5-5'-CCTAGCAGGTGCAGTGG-3'.

We calculate the distance d_{DA} between Cy3 donor and Cy5 using the formula for standard B form DNA $d_{DA} = (L-1) \times H + D$ where L is the length of the helix in base pairs, $H = 0.34$ nm

is the helical rise per base pair step, and $D = 0.8$ nm is the additional axial separation for the two fluorophores including the linker length. The Förster radius is $R_0 = 60$ Å for Cy3-Cy5.[11]

For the Atto550-20-Atto647N sample, we use the same sequence of 51 base pairs length as in our previous work carrying one Atto550 donor on the forward strand, and one Atto647N acceptor on the reverse strand, with a 20 base pair separation between the dyes.[42] The Förster radius is 65 Å for Atto550-Atto647N.[40] The sequences for the Atto550-20-Atto647N sample are:

5' CCTGAGCGTACTGCAGGATAGCCTATCGCGTGTCATATGCTGT$\mathbf{T_D}$CAGTGCG 3',

5' CGCACTGAACAGCATATGACACGCGA$\mathbf{T_A}$AGGCTATCCTGCAGTACGCTCAGG 3'.

Labeled HPLC-purified DNA single strands are obtained from IBA (Göttingen, Germany). Cy3 and Cy5 fluorophores are directly linked to cytosine at the 5'- terminus during oligonucleotide synthesis via a three atom carbon linker. Atto550 and Atto647N dyes are covalently linked to an amino-C6-modified thymidine with NHS-chemistry via base labeling. The reference sequences carrying only the isolated donor or acceptor are constructed with unlabeled complementary strand respectively. The single strands are annealed at 10 μM concentration in 20 mM Tris, 1 mM EDTA, 500 mM NaCl, 12 mM $MgCl_2$ buffer, and by heating to 95°C for 5 min followed by slow cooling to room temperature. Double stranded DNA stocks are diluted in a 10 mM Hepes-NaOH buffer, pH 7.5 (Sigma-Aldrich).

Experimental setup. Experiments recording simultaneously the donor and the acceptor emission photodynamics are performed on a confocal inverted microscope with a Zeiss C-Apochromat 63x 1.2NA water-immersion objective. The excitation source is a iChrome-TVIS laser (Toptica GmbH) delivering 3 ps pulses at 40 MHz repetition rate and 550 nm wavelength. The laser beam has a waist of 300 nm at the focal spot of the 1.2NA objective. We use a nanomolar concentration for the confocal reference, 250 nM for the nanoaperture and 5 μM for the nanoantenna so that the average number of FRET construct within the observation volume is less than one in each case.[41,42] The average excitation power is set to 10 μW, well within the linear regime for the excitation of the fluorescent dyes.[42] The illumination conditions correspond to 0.035 mW/μm^2 power density leading to a maximum temperature increase lesser than 2 °C. The laser excitation is fil-

tered by a set of two bandpass filters (Chroma ET525/70M and Semrock FF01-550/88). Dichroic mirrors (Chroma ZT594RDC and ZT633RDC) separate the donor and acceptor fluorescence from the reflected laser light. The detection is performed by two avalanche photodiodes (Micro Photon Devices MPD-5CTC with < 50 ps timing jitter) with 620 ± 20 nm (Chroma ET605/70M and ET632/60M) and 670 ± 20 nm (Semrock FF01-676/37) fluorescence bandpass filters for the donor and acceptor channels respectively. The photodiode signal is recorded by a fast time-correlated single photon counting module (Hydraharp400, Picoquant GmbH) in time-tagged time-resolved (TTTR) mode. Each trace duration is typically 200 s. The temporal resolution for fluorescence lifetime measurements is 37 ps at half-maximum of the instrument response function.

FRET efficiency analysis. For each detected fluorescence burst, the number of detected photons in the acceptor channel n_a and in the donor channel n_d are recorded, and the FRET efficiency is computed according to the formula:[40]

$$E_{FRET} = \frac{n_a - \alpha n_d - n_{ao}^{de}}{n_a - \alpha n_d - n_{ao}^{de} + \gamma n_d} \tag{1}$$

This analysis takes into account several additional effects to avoid artifacts: the donor emission crosstalk into the acceptor channel, the direct excitation of the acceptor by the laser light, and the difference in the quantum yields and detection efficiencies of the donor and acceptor emission. In the above expression, α is the crosstalk parameter defined as the ratio of isolated donor fluorescence falling into the acceptor detection channel as compared to the signal detected in the donor channel. We experimentally measure α from the intensity levels obtained with the isolated donor on both detectors, and find $\alpha = 0.18$ for Cy3 in the confocal setup and in the nanoaperture, and $\alpha = 0.22$ for Cy3 in the aluminum nanogap antenna. n_{ao}^{de} is the number of detected photons resulting from the direct excitation of the Cy5 acceptor dye by the laser light. This parameter is carefully measured for every antenna by recording the average number of detected photons per burst when only the acceptor dye is present. Lastly, $\gamma = \kappa_a \phi_a / \kappa_d \phi_d$ accounts for the differences in quantum yields (ϕ_a and ϕ_d) and fluorescence detection efficiencies (κ_a and κ_d) between the ac-

ceptor and donor. We estimate $\gamma_{ref} = 2.3$ for the confocal reference on Cy3-Cy5 samples. For the plasmonic structures, the ratio γ is increased by the ratio of the fluorescence enhancement factors $\eta_{F,a}$ and $\eta_{F,d}$ for the isolated acceptor and isolated donor: $\gamma_{ant} = \gamma_{ref}\eta_{F,a}/\eta_{F,d}$ since both acceptor and donor dyes undergo the same excitation intensity enhancement. For the aperture, the ratio becomes $\gamma_{ant} = 2.47$ using the fluorescence enhancement factors $\eta_{F,a} = 5.75$ and $\eta_{F,d} = 5.4$ obtained from fluorescence correlation spectroscopy analysis for isolated Cy3 and Cy5 terminally attached to double stranded DNA.[41] For the antenna, we find $\gamma_{ant} = 1.73$ according to the fluorescence enhancement factors $\eta_{F,a} = 7.8$ and $\eta_{F,d} = 10.6$ again calibrated from fluorescence correlation spectroscopy.[42] The full trace analysis is implemented using the software Symphotime 64 (Picoquant GmbH).

Fluorescence lifetime analysis. The time correlated single photon counting (TCSPC) histograms are fitted using Levenberg-Marquard optimization, implemented using the commercial software Symphotime 64 (Picoquant GmbH) and taking into account the reconvolution by the instrument response function (IRF). The time interval for fit is set to ensure that more than 85% of the detected count events are taken into account in the region of interest. The Cy3 donor fluorescence decays are fitted with a triple exponential model, which was already found necessary for the confocal case following the approach in Ref.[11] In contrast to gold nanostructures, aluminum-based antennas do not yield noticeable photoluminescence, so that there is no fast sub-5 ps contribution on the fluorescence decays that would originate from the metal photoluminescence.[41,42] We then use the amplitude-averaged fluorescence lifetime to compare between the experiments (all fitting parameters are summarized in the Supporting Information Tab. S1). The FRET rate is obtained as $\Gamma_{FRET} = \Gamma_{DA} - \Gamma_{Do} = 1/\tau_{DA} - 1/\tau_{Do}$, where τ_{DA} and τ_{Do} are the amplitude-averaged donor lifetime in the presence and absence of the acceptor respectively. The FRET efficiency is deduced as $E_{FRET} = 1 - \Gamma_{Do}/\Gamma_{DA} = 1 - \tau_{DA}/\tau_{Do}$.

Numerical simulations. Electric field distributions are computed using finite-difference time-domain FDTD method (RSoft Fullwave software) with a mesh size of 1 nm. The antenna parameters are set to reproduce the fabricated devices, with a hemispherical shape of the 80 nm aluminum

nanoparticle and 20 nm gap. For the dipole emission, the wavelength is 600 nm, and the aluminum permittivity is taken from.[63]

Supporting Information

FRET efficiency histograms in the reference confocal setup, Fluorescence spectra confirm the occurrence of FRET in the Cy3-Cy5 constructs, Fluorescence absorption and emission spectra for the donor and acceptor dyes, Supplementary time trace on Cy3-12-Cy5 FRET sample, Reference FRET histograms for isolated Cy3 donor (no energy transfer), Table of fluorescence lifetimes and fitting parameters for time-correlated fluorescence decays, FRET rate constants for Cy3-Cy5 constructs, Comparison of FRET efficiencies using the two measurement methods. This material is available free of charge *via* the Internet at http://pubs.acs.org.

Additional information

The authors declare no competing financial interests.

Acknowledgments

The research leading to these results has received funding from the European Commission's Seventh Framework Programme (FP7-ICT-2011-7) under grant agreements ERC StG 278242 (ExtendFRET), 288263 (NanoVista) and ERC AdG 247330 (Nano Antennas).

References

(1) Förster, T. *Ann. Phys.* **1948**, *437*, 55-75.

(2) Roy, R.; Hohng, S.; Ha, T. *Nat. Methods* **2008**, *5*, 507-516.

(3) Kühlbrandt, W.; Wang, DN. *Nature* **1991**, *350*, 130-134.

(4) Hardin, B. E.; Hoke, E. T.; Armstrong, P. B.; Yum, J. H.; Comte, P.; Torres, T.; Fréchet, J. M. J.; Nazeeruddin, M. K.; Grätzel, M.; McGehee, M. D. *Nat. Photonics* **2009**, *3*, 406-411.

(5) Baldo, M.A.; Thompson, M.E.; Forrest S.R. *Nature* **2000**, *403*, 750-753.

(6) Deniz, A.A.; Dahan, M.; Grunwell, J.R.; Ha, T.; Faulhaber, A.E.; Chemla, D.S.; Weiss, S.; Schultz P.G. *Proc. Natl. Acad. Sci.* **1999**, *96*, 3670-3675.

(7) Weiss S. *Nat. Struct. Biol.* **2000**, *7*, 724-729.

(8) Schuler, B.; Lipman, E. A.; Eaton, W. A. *Nature* **2002**, *419*, 743-747.

(9) Medintz, I. L.; Clapp, A. R.; Mattoussi, H.; Goldman, E. R.; Fisher, B.; Mauro, J. M. *Nat. Mater.* **2003**, *2*, 630-638.

(10) Lewis, F. D.; Zhang, L.; Zuo, X. *J. Am. Chem. Soc.* **2005**, *127*, 10002-10003.

(11) Iqbal, A.; Arslan, S.; Okumus, B.; Wilson, T. J.; Giraud, G.; Norman, D. G.; Ha, T.; Lilley, D. M. J. *Proc. Natl. Acad. Sci. U. S. A.* **2008**, *105*, 11176-11181.

(12) Rindermann, J. J.; Akhtman, Y.; Richardson, J.; Brown, T.; Lagoudakis, P. G. *J. Am. Chem. Soc.* **2011**, *133*, 279-285.

(13) Sindbert, S.; Kalinin, S.; Nguyen, H.; Kienzler, A.; Clima, L.; Bannwarth, W.; Appel, B.; Müller, S.; Seidel, C. A. *J. Am. Chem. Soc.* **2011**, *133*, 2463-2480.

(14) Novotny, L.; van Hulst, N. *Nat. Photonics* **2011**, *5*, 83-90.

(15) Giannini, V.; Fernandez-Dominguez, A. I.; Heck, S. C.; Maier, S. A. *Chem. Rev.* **2011**, *111*, 3888–3912.

(16) Andrew, P.; Barnes, W.L. *Science* **2000**, *290*, 785-788.

(17) Finlayson, C. E.; Ginger, D. S.; Greenham, N. C. *Chem. Phys. Lett.* **2001**, *338*, 83-87.

(18) Zhong, X.; Chervy, T.; Wang, S.; George, J.; Thomas, A.; Hutchison, J. A.; Devaux, E.; Genet, C.; Ebbesen, T. W. *Angew. Chem. Int. Ed.* **2016**, *55*, 6202-6206.

(19) Govorov, A. O.; Lee, J.; Kotov, N. A. *Phys. Rev. B* **2007**, *76*, 125308.

(20) Vincent, R.; Carminati, R. *Phys. Rev. B* **2011**, *83*, 165426.

(21) Pustovit, V. N.; Shahbazyan, T. V. *Phys. Rev. B* **2011**, *83*, 085427.

(22) Faessler, V.; Hrelescu, C.; Lutich, A. A.; Osinkina, L.; Mayilo, S.; Jäckel, F.; Feldmann, J. *Chem. Phys. Lett.* **2011**, *508*, 67-70.

(23) Zhao, L.; Ming, T.; Shao, L.; Chen, H.; Wang, J. *J. Phys. Chem. C* **2012**, *116*, 8287-8296.

(24) Gonzaga-Galeana, J. A.; Zurita-Sánchez, J. R. *J. Chem. Phys.* **2013**, *139*, 244302.

(25) Marocico, C. A.; Zhang, X.; Bradley, A. L. *J. Chem. Phys.* **2016**, *144*, 024108.

(26) Andrew, P.; Barnes, W.L. *Science* **2004**, *306*, 1002-1005.

(27) Bouchet, D.; Cao, D.; Carminati, R.; De Wilde, Y.; Krachmalnicoff, V. *Phys. Rev. Lett.* **2016**, *116*, 037401.

(28) de Roque, P. M.; van Hulst, N. F.; Sapienza, R. *New J. Phys.* **2015**, *17*, 113052.

(29) de Torres, J.; Ferrand, P.; Colas des Francs, G.; Wenger, J. *ACS Nano* **2016**, *10*, 3968-3976.

(30) Blum, C.; Zijlstra, N.; Lagendijk, A.; Wubs, M.; Mosk, A. P.; Subramaniam, V.; Vos, W. L. *Phys. Rev. Lett.* **2012**, *109*, 203601.

(31) Tumkur, T.; Kitur, J.; Bonner, C.; Poddubny, A.; Narimanov, E.; Noginov, M. *Faraday Discuss.* **2015**, *178*, 395-412.

(32) Wubs, M.; Vos, W. L. *New J. Phys.* **2016**, *18*, 053037.

(33) Schleifenbaum, E.; Kern, A. M.; Konrad, A.; Meixner, A. J. *Phys. Chem. Chem. Phys.* **2014**, *16*, 12812-12817.

(34) Konrad, A.; Metzger, M.; Kern, A.M.; Brecht M.; Meixner, A.J. *Nanoscale* **2015**, *7*, 10204-10209.

(35) de Dood, M. J. A.; Knoester, J.; Tip, A.; Polman, A. *Phys. Rev. B* **2005**, *71*, 115102.

(36) Rabouw, F. T.; den Hartog, S. A.; Senden, T.; Meijerink, A. *Nat. Commun.* **2014**, *5*, 3610.

(37) Lunz, M.; Gerard, V. A.; Gun´ko, Y. K.; Lesnyak, V.; Gaponik, N.; Susha, A. S.; Rogach, A.L.; Bradley, A. L. *Nano Lett.* **2011**, *11*, 3341-3345.

(38) Zhang, X.; Marocico, C. A.; Lunz, M.; Gerard, V. A.; Gun´ko, Y. K.; Lesnyak, V.; Gaponik, N.; Susha, A.S.; Rogach, A.L.; Bradley, A. L. *ACS Nano* **2011**, *6*, 9283-9290.

(39) Zhang, X.; Marocico, C. A.; Lunz, M.; Gerard, V. A.; Gun´ko, Y. K.; Lesnyak, V.; Gaponik, N.; Susha, A.S.; Rogach, A.L.; Bradley, A. L. *ACS Nano* **2014**, *8*, 1273-1283.

(40) Ghenuche, P.; de Torres, J.; Moparthi, S. B.; Grigoriev, V.; Wenger, J. *Nano Lett.* **2014**, *14*, 4707-4714.

(41) de Torres, J.; Ghenuche, P.; Moparthi, S. B.; Grigoriev, V.; Wenger, J. *Chem. Phys. Chem.* **2015**, *16*, 782-788.

(42) Ghenuche, P.; Mivelle, M.; de Torres, J.; Moparthi, S. B.; Rigneault, H.; Van Hulst, N. F.; Garcia-Parajo, M. F.; Wenger, J. *Nano Lett.* **2015**, *15*, 6193–6201.

(43) Bidault, S.; Devilez, A.; Ghenuche, P.; Stout, B.; Bonod, N.; Wenger, J. *ACS Photonics* **2016**, *3*, 895-903.

(44) Novotny, L.; Hecht, B. *Principles of Nano-Optics.* Cambridge University Press, Cambridge, **2006**.

(45) Norman, D. G.; Grainger, R. J.; Uhrín, D.; Lilley, D. M. J. *Biochemistry* **2000**, *39*, 6317-6324.

(46) Iqbal, A.; Wang, L.; Thompson, K. C.; Lilley, D. M. J.; Norman, D. G. *Biochemistry* **2008**, *47*, 7857-7862.

(47) Ouellet, J.; Schorr, S.; Iqbal, A.; Wilson, T. J.; Lilley, D. M. J. *Biophys. J.* **2011**, *101*, 1148-1154.

(48) Spiriti, J.; Binder, J. K.; Levitus, M.; Van der Vaart, A. *Biophys. J.* **2011**, *100*), 1049-1057.

(49) Sanborn, M.E.; Connolly, B. K.; Gurunathan, K.; Levitus, M. *J. Phys. Chem. B* **2007**, *111*, 11064-11074.

(50) Regmi, R.; Al Balushi, A. A.; Rigneault, H.; Gordon, R.; Wenger, J. *Sci. Rep.* **2015**, *5*, 15852.

(51) Kinkhabwala, A.; Yu, Z. F.; Fan, S. H.; Avlasevich, Y.; Mullen, K.; Moerner, W. E. *Nat. Photonics* **2009**, *3*, 654-657.

(52) Acuna, G. P.; Möller, F. M.; Holzmeister, P.; Beater, S.; Lalkens, B.; Tinnefeld, P. *Science* **2012**, *338*, 506–510.

(53) Punj, D.; Mivelle, M.; Moparthi, S.B.; van Zanten, T.S.; Rigneault, H.; van Hulst, N.F.; García-Parajó, M.F.; Wenger, J. *Nat. Nanotechnol.* **2013**, *8*, 512–516.

(54) Khatua, S.; Paulo, P. M.; Yuan, H.; Gupta, A.; Zijlstra, P.; Orrit, M. *ACS Nano* **2014**, *8*, 4440–4449.

(55) Akselrod, G. M.; Argyropoulos, C.; Hoang, T. B.; Ciracì, C.; Fang, C.; Huang, J.; Smith, D. R.; Mikkelsen, M. H. *Nat. Photonics* **2014**, *8*, 835–840.

(56) Hoang, T. B.; Akselrod, G. M.; Mikkelsen, M. H. *Nano Lett.* **2016**, *16*, 270-275.

(57) Bidault, S.; Devilez, A.; Maillard, V.; Lermusiaux, L.; Guigner, J.-M.; Bonod, N.; Wenger, J. *ACS Nano* **2016**, *10*, 4806–4815.

(58) Curto, A. G.; Volpe, G.; Taminiau, T. H.; Kreuzer, M. P.; Quidant, R.; van Hulst, N. F. *Science* **2010**, *329*, 930–933.

(59) Pellegrotti, J. V.; Acuna, G. P.; Puchkova, A.; Holzmeister, P.; Gietl, A.; Lalkens, B.; Stefani, F. D.; Tinnefeld, P. *Nano Lett.* **2014**, *14*, 2831-2836.

(60) Wientjes, E.; Renger, J.; Cogdell, R. J.; van Hulst, N. F. *J. Phys. Chem. Lett.* **2016**, *7*, 1604-1609.

(61) Holzmeister, P.; Acuna, G.P.; Grohmann, D.; Tinnefeld, P. *Chem. Soc. Rev.* **2013**, *43*, 1014-1028.

(62) Punj, D.; Ghenuche, P.; Moparthi, S. B.; de Torres, J.; Grigoriev, V.; Rigneault, H.; Wenger, J. *WIREs Nanomed. Nanobiotechnol.*, **2014**, *6*, 268-282.

(63) McPeak, K. M.; Jayanti, S. V.; Kress, S. J.; Meyer, S.; Iotti, S.; Rossinelli, A.; Norris, D. J. *ACS Photonics* **2015**, *2*, 326-333.

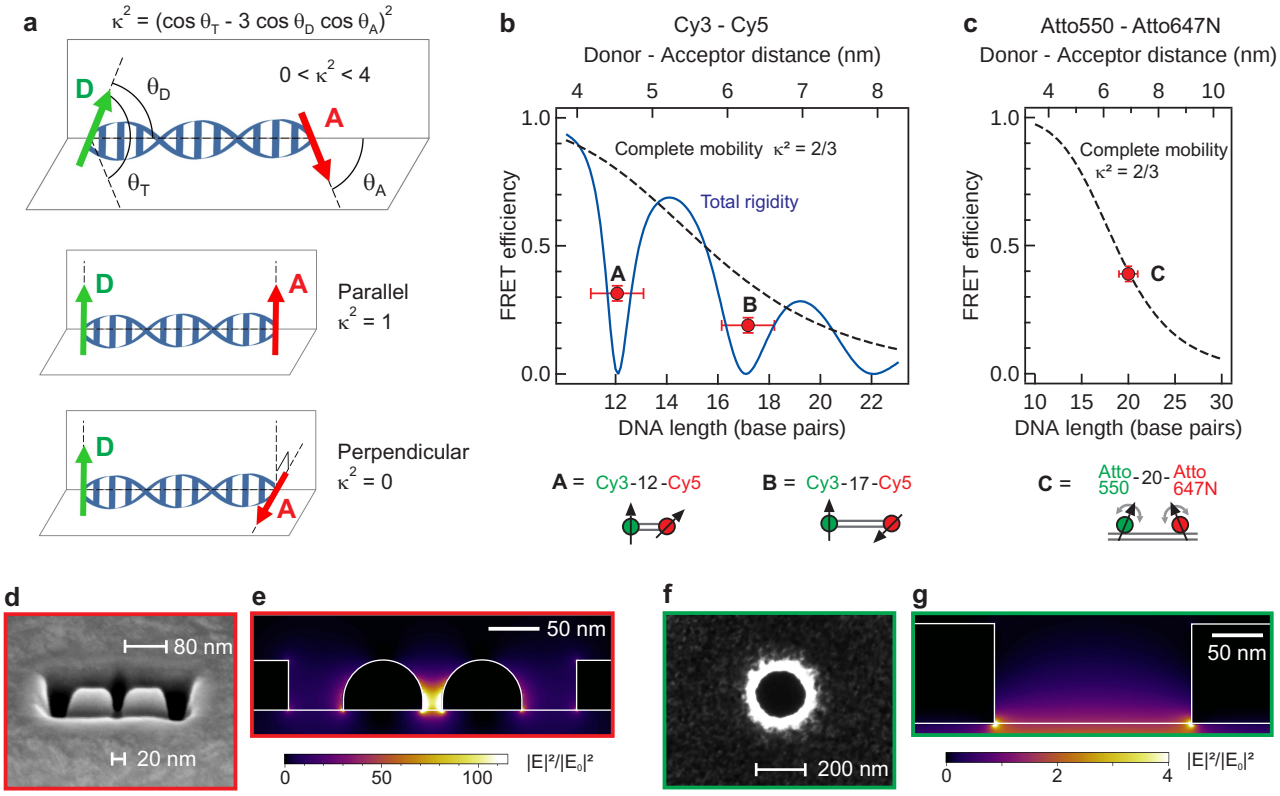

Figure 1: FRET constructs and plasmonic nanostructures to enhance energy transfer. (a) Definition of the FRET orientation parameter κ^2 between a donor (D) and an acceptor (A) dipole. The lower panels show the simplified cases when both dipoles are in parallel planes with colinear (κ^2=1) or perpendicular (κ^2=0) orientations. (b) Simulated evolution of the FRET efficiency between Cy3 and Cy5 terminally attached to duplex DNA as a function of the length of the DNA helix. The calculations show the extreme cases of total rigidity of the fluorophores stacked on the DNA (blue line) and complete mobility (black dashed line) corresponding to the orientation-averaged $\kappa^2 = 2/3$. The experimental data (red dots) for the constructs using 12 and 17 base pair separations validate the predominant stacking of the Cy3 and Cy5 fluorophores on the ends of the DNA helix in near perpendicular orientations. (c) Same as (b) for the Atto550-Atto647N system which serves as a reference for the complete orientational mobility of the fluorophores. (d) Scanning electron microscope image of a nanogap antenna milled in an aluminum film. (e) Excitation intensity enhancement computed at 550 nm with horizontal excitation polarization along the nanogap. (f,g) Same as (e,f) for a 200 nm diameter aperture milled in aluminum.

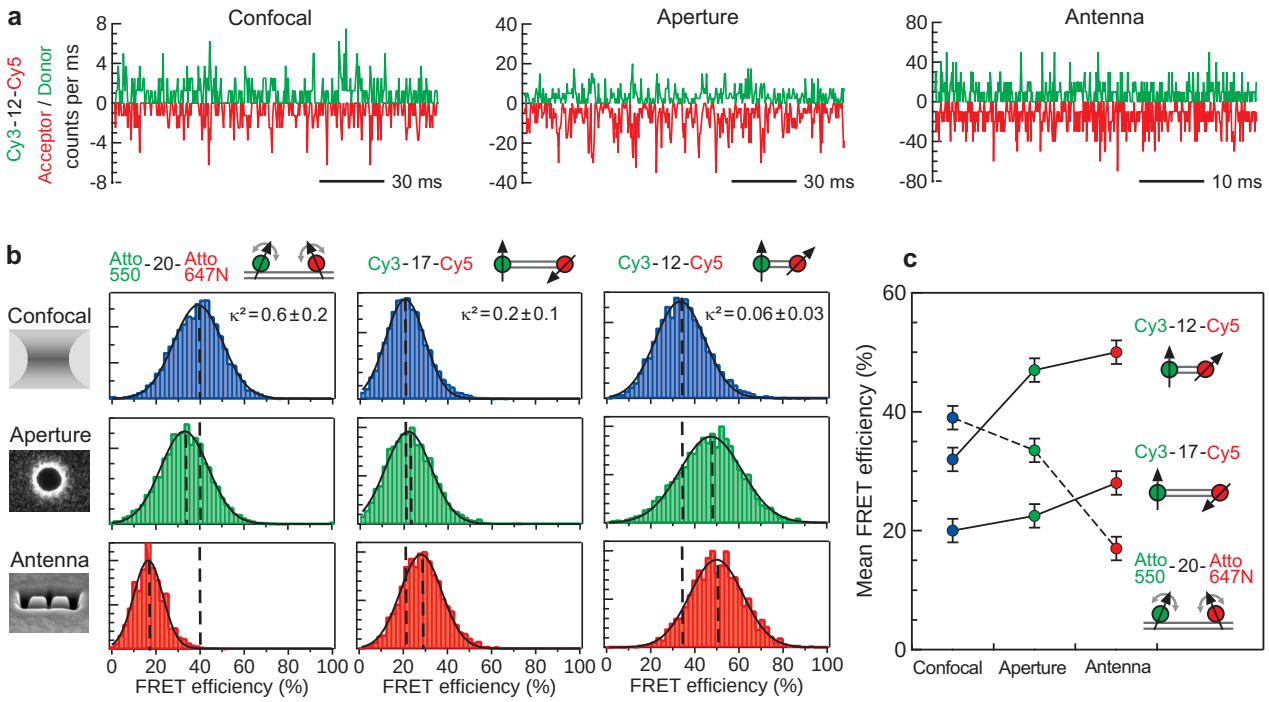

Figure 2: FRET efficiency enhancement in aluminum nanostructures. (a) Fluorescence time traces for the donor (green) and acceptor (red, inverted vertical axis) detection channels for the Cy3-12-Cy5 sample (donor with the acceptor at 12 base pairs separation) on the confocal reference, the 200 nm diameter aperture and the 20 nm gap antenna (note the different vertical scalings). The binning time is 0.4 ms for the confocal and aperture cases and 0.1 ms for the antenna. All count rates are computed back in counts per millisecond for direct comparison between the bursts amplitudes. Longer traces of 20 s duration are provided in the Supporting Information Fig. S4. (b) Comparison of the FRET efficiency histograms for the different constructs and configurations: confocal, 200 nm diameter aperture and 20 nm gap antenna. κ^2 is the orientation parameter measured for the confocal setup. Black lines are Gaussian fits used to determine and compare the mean FRET efficiencies (indicated by dashed vertical lines). (c) Evolution of the mean FRET efficiency in the different configurations. The error bars correspond to the standard error on the mean plus a term to take into account potential systematic deviations in the FRET efficiency computation.

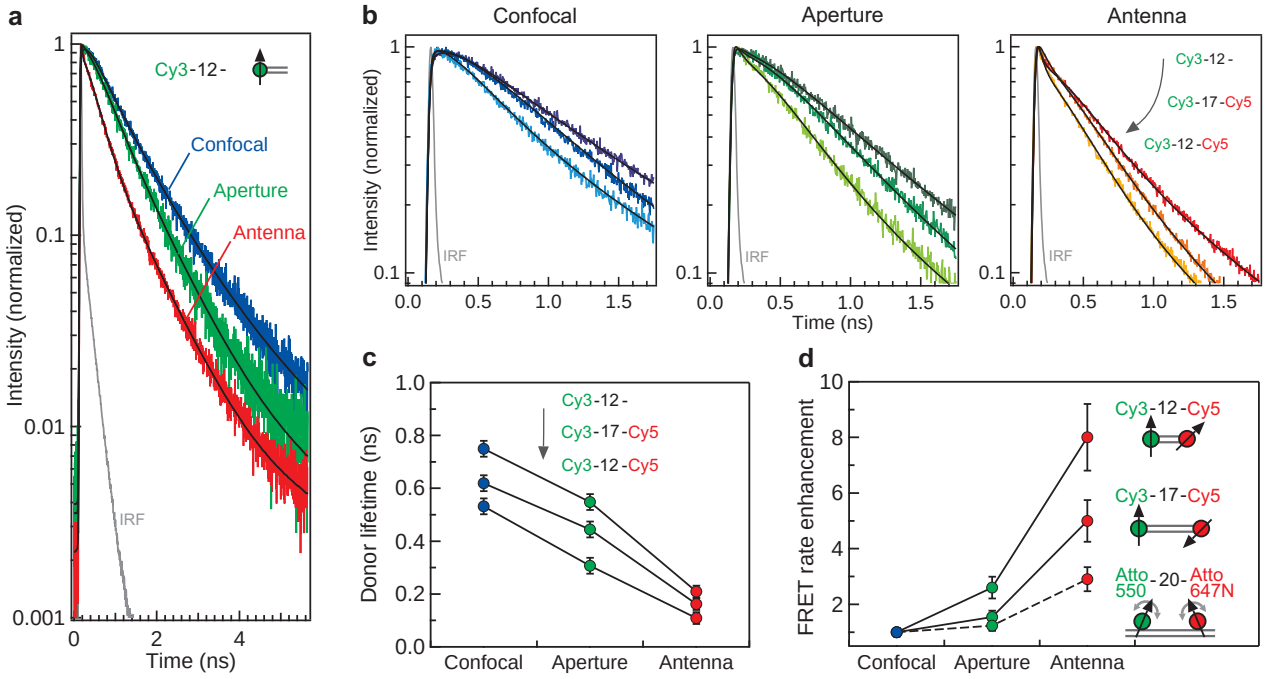

Figure 3: Accelerated donor photodynamics confirm FRET efficiency enhancement. (a) Comparison of the normalized fluorescence decay traces for the isolated Cy3 donor conjugated to DNA in the confocal, aperture and antenna setup (no acceptor in this case). Black lines are numerical fits convoluted by the instrument response function (IRF, grey curve). The acceleration of the donor photodynamics demonstrates an enhanced local density of optical states (LDOS) in the aperture and even more pronounced in the nanoantenna. (b) Normalized fluorescence decay traces for the Cy3 donor in presence of the acceptor. For each subgraph, from top to bottom, the curves correspond to the isolated donor on 12 base pairs DNA (Cy3-12-), the donor with the acceptor at 17 base pairs separation (Cy3-17-Cy5) and the donor with the acceptor at 12 base pairs separation (Cy3-12-Cy5). For each confocal, aperture and antenna case, the acceptor proximity accelerates the donor photodynamics and demonstrates the occurrence of FRET. Black lines are numerical fits convoluted by the IRF. (c) Average donor fluorescence lifetime deduced from the traces in (a,b). From top to bottom, the curves correspond to the Cy3 donor without the acceptor (Cy3-12-) and with the presence of the acceptor at 17 base pairs separation (Cy3-17-Cy5) and 12 base pairs separation (Cy3-12-Cy5). (d) Enhancement factors for the FRET rate constant Γ_{FRET} computed with respect to the confocal reference.

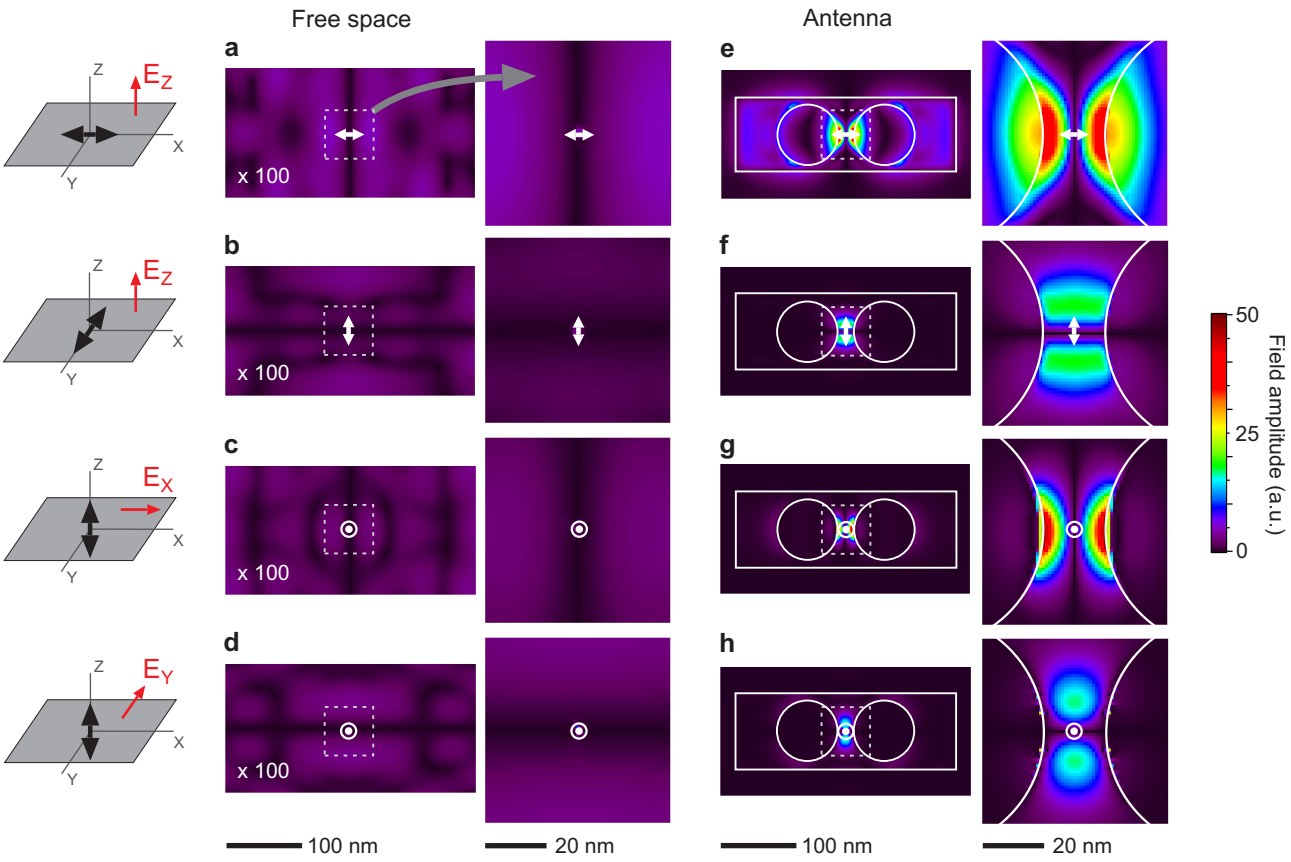

Figure 4: Spatial distributions of the electric field amplitude emitted by a point dipolar source in free space (a-d) and in the center of a 20 nm gap nanoantenna (e-h). The schemes on the left column indicate the dipole orientation (black arrow), the plane of view (gray) and the component of the electric field (red) that is displayed. For the free space references (a-d), the field amplitude is near zero as we select the azimuthal component. To ease viewing on the same colorscale for all sub images, the field amplitude has been multiplied by 100x for the free space cases (a-d). The dipole positions and orientations are again indicated on the images as white arrows. The dashed squares on the images represent the zones which are magnified on the right column.